

FRACTURE CHARACTERIZATION AND SEM EXAMINATION
OF NAPTF CC6 CONCRETE MIXES

By:

Shelley Stoffels, Maria Lopez, Lin Yeh, Yoseok Jeong,
Saman Barzegari and Behnoud Kermani
The Thomas D. Larson Pennsylvania Transportation Institute
The Pennsylvania State University
3127 Research Drive
University Park, PA 16802
USA

Phone: (814) 865-7254

sms26@engr.psu.edu

mmlopez@engr.psu.edu

PRESENTED FOR THE
2014 FAA WORLDWIDE AIRPORT TECHNOLOGY TRANSFER CONFERENCE
Galloway, New Jersey, USA

August 2014

INTRODUCTION

The Federal Aviation Administration (FAA) rigid pavement design procedure utilizes the flexural strength to stress ratio to predict performance, based on regression models developed from full-scale experiments by the Corps of Engineers and FAA (1). Construction Cycle 6 (CC6) at the National Airport Pavement Test Facility (NAPTF) was constructed to further examine the effects of concrete strength on structural performance through full-scale accelerated testing. For CC6, FAA utilized concrete mixtures with three target flexural strengths. To complement the full-scale accelerated testing, both lab-cured and field-sawn beams were tested. Beam strength and fatigue tests were performed in the FAA testing lab. Fracture properties of the three design mixtures were determined at the PSU laboratory following RILEM TC-187-SOC (Planas, 2). Scanning Electron Microscopy was conducted to investigate the micro-structural differences between concrete samples to investigate apparent anomalies in other laboratory observations.

BACKGROUND

The FAA researchers at the NAPTF cast 6 x 6 x 21-in beams from each of the three concrete mixes (different flexural strengths) used for CC6, and also obtained sawn beams from the slabs at the conclusion of the full-scale accelerated testing. The FAA has performed in-house laboratory testing of these beams for flexural strength and fatigue. In particular, the beams were tested at a number of stress levels, including those producing very low numbers of cycles to failure. As shown in Table 1, the three CC6 mixes include differences in coarse aggregate source, sand source and quantity, cement content, air content, slump, and water/cement ratio. Because the three mixes differ in a number of parameters, in addition to flexural strength, it is postulated that there may be confounding factors affecting the correlation of flexural strength to fatigue strength. While the mix parameters and variability have been carefully documented, it was desired to obtain additional properties that may be correlated to fatigue and field performance. In June 2012, FAA delivered 18 beams and 18 concrete cores (lab-cured specimens) to Penn State for fracture characterization.

Table 1.
FAA NAPTF CC6 Mix Designs.

Material (relative target flexural strength)	MRS1 (low)	MRS2 (medium)	MRS3 (high)
Target Strength (modulus of rupture), psi	500	750	1000
Harmony No. 57 Stone, Round, lbs	1550		
No. 57 Coarse Aggregate, lbs		1475	1535
No. 8 Intermediate Coarse Aggregate, lbs		490	535
Harmony Concrete Sand, lbs	1414		
Concrete Sand, lbs		1225	1070
Water, lbs	325	230	236
Type 1 Portland Cement, lbs	460	500	680
Air, %	6.5	7	4.5
Slump, in.	6	5.5	3.5
SIKAair, oz.	4.5	5	4.5
w/c Ratio	0.71	0.46	0.35

Anomalous results were observed by FAA in the routine strength testing of the beam samples from CC6. After approximately two years of moist curing, the beams from MRS2 and MRS3 were found to have average flexural strengths lower than the 28-day strengths, as documented by Stein (3). After the conclusion of the CC6 accelerated testing, beams were sawn from the full-scale test sections. Stein (3) found that the average flexural strengths of the sawn beams were approximately the same as the 28-day strengths for all three concrete mixtures.

In November 2012, 10 beams and 10 concrete cores, sawn from the accelerated testing slabs, were collected from the FAA NAPTF facility for fracture characterization at Penn State. A third set of specimens, 14 beams and 14 cores of field-sawn specimens, were delivered to Penn State's CITEL facility on March 2013. After arrival at the Penn State lab, all specimens were stored in the curing room at 23°C and 95% relative humidity until the time of testing.

FRACTURE AND SPLIT TENSILE TESTING OF CC6 SPECIMENS

Research work on concrete fatigue crack growth has identified that the empirical Paris law can be applied to concrete. Bazant and Xu (4) and Bazant and Schell (5) modified this law to account for the size-effect of the specimens. Their results indicate that the fracture process zone for a specimen subjected to fatigue loading (for the same load amplitude) is likely to be larger than for a specimen subjected to monotonic loading, this effect was found to be more pronounced in normal concrete than for high strength concrete. But that also means that fatigue of larger-size specimens or structures can be predicted using a strength limit approach. In the paper by Bazant and Xu, they show that size effect happens with smaller specimens. The size effect on bending fatigue was also discussed by Zhang (6).

Finding fracture energy parameters and correlating them to the flexural strength may be feasible. It also appears that cyclic loading behavior can be correlated with monotonic testing, so if the fracture energy of the material is known, you could numerically model the cyclic behavior and thus predict failure (assuming estimated stress levels or at load path) (Shah, 7). Toumi and Bascoul (8) modeled fatigue behavior with a relative level of success, using the fracture energy of the concrete. The authors posed further questions, similar to those relevant to concrete airfield pavement fatigue, regarding the applicability to different load levels and mixes.

Fracture Tests of CC6 Mixes

Using the cast lab-cured beams, split tensile tests and three-point bending tests of notched beams were conducted during the summer of 2012. The splitting tensile (Brazilian) tests followed ASTM C496; results are included in Table 2. Recommendations regarding the width of the bearing strip as provided by Rocco et al. (9) were used. Three-point bending tests were performed in a closed-loop machine using CMOD control (crack-mouth opening displacement). For this test protocol, beams are notched prior to testing; notch geometry (depth and width) follows RILEM recommendations, Planas (2). Figure 1 shows typical load-CMOD and load-PLD (point load displacement) curves for the lab-cured beams. The resulting fracture energy values are presented in Table 2. The total fracture energy is labeled as G_F ; the size-effect fracture energy is G_f (Bazant and Schell, 5).

Concrete fracture energies and split tensile strengths were also obtained for the field-sawn specimens; the results are presented in Table 3.

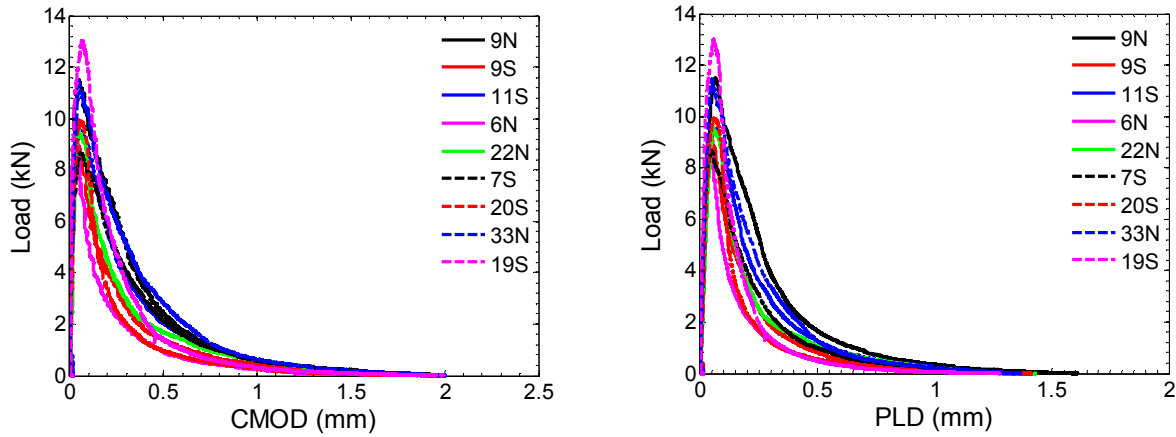


Figure 1. Typical Load-CMOD and Load-PLD curves from lab-cured specimens

Table 2.

Summary of Three-Point Bending and Split Tensile Test Results for Cast Lab-Cured Specimens.

Location	Slab ID	Test Date	Peak Load (kN)	Elastic Modulus (GPa)	G_F (N/m)	G_f (N/m)	f_i (MPa)
MRS1	6N	8/24/2012	9.1	43.55	111	40 ^a	2.62
MRS1	22S	8/27/2012	9.58	40.66	180	35	3.3
MRS1	20S	8/28/2012	9.92	52.14	129	32	3.3
MRS1	24N	8/30/2012	9.34	30.43	138	49	3.16
MRS1	4N	9/5/2012	10.4	35.56	114	73	2.82
MRS1	4S	9/5/2012	10.21	30.49	106	79	2.82
MRS2	9N	8/23/2012	11.5	44.59	258	106	2.79
MRS2	9S	8/23/2012	9.24	51.1	171	24	3.04
MRS2	11S	8/24/2012	9.52	45.49	231	47	2.52
MRS2	7S	8/27/2012	8.67	41.32	211	39	2.68
MRS2	11N	8/31/2012	9.19	38.97	160	26	3.69
MRS2	29N	8/30/2012	9.39	44.09	168	25 ^b	3.23
MRS3	33N	8/28/2012	11.45	54.02	245	56	3.22
MRS3	19S	8/29/2012	13.03	60.88	161	103	3.17
MRS3	17S	8/29/2012	11.18	131.39	213	18	3.26
MRS3	17N	8/31/2012	11.13	44.39	249	62	3.26
MRS3	15N	9/2/2012	8.31	46.28	158	16	3.61
MRS3	15S	9/4/2012	10.57	206.9	236	9	3.43

a: Elastic modulus was obtained by calculating the slope between 35% and 75% of peak load on the ascending branch of CMOD (crack mouth opening displacement)-load curve. (all other specimens use RILEM procedure: 15% and 55% of peak load)

b: Elastic modulus was obtained by calculating the slope of LPD (load point displacement)-load curve (between 15% and 55% of peak load).

Table 3.
Summary of Three-Point Bending and Split Tensile Test Results for Field-Sawn Specimens.

Location	Specimen ID	Test Data	Peak Load (kN)	Elastic Modulus (GPa)	G_F (N/m)	G_f (N/m)	f_t (MPa)
MRS1	4N-1 ^a	4/2/2013	7.6	25.95	92	33 ^a	2.64
MRS1	4N-2	4/2/2013	9.39	32.33	119	62	
MRS1	22S-1	4/3/2013	9.08	37.11	64	29 ^b	2.63
MRS1	22S-2	4/3/2013	9.45	40.43	90	33 ^b	
MRS1	6S-1	7/23/2013	8.96	32.31	101	56	2.49
MRS1	6S-2	7/22/2013	7.99	41.44	66	26	
MRS1	20N-1	7/24/2013	8.16	39.72	98	27	2.62
MRS1	20N-2	7/23/2013	7.74	40.6	81	22	
MRS2	29S-1	1/12/2013	11.31	44.68	138	48	3.22
MRS2	29S-2	1/12/2013	10.96	42.92	205	29	
MRS2	31S-1	1/14/2013	9.5	18.46	112	67	3.22
MRS2	31S-2	1/14/2013	8.62	55.99	85	15	
MRS2	13N-1	4/25/2013	8.16	35.02	135	23	2.78
MRS2	13N-2	4/25/2013	7.99	40.53	166	23	
MRS2	7N-1	7/24/2013	8.31	56.32	137	31	2.24
MRS2	7N-2	7/25/2013	6.96	34.4	149	24	
MRS3	15N-1	1/11/2013	12.56	49.87	128	115	2.88
MRS3	15N-2	1/11/2013	12.24	58.17	95	56	
MRS3	17N-1	1/18/2013	10.77	62.9	101	27	3.37
MRS3	17N-2	1/16/2013	12.78	79.63	131	55	
MRS3	35S-1	1/10/2013	11.13	45.83	104	55	3.69
MRS3	35S-2	1/10/2013	12.34	58.74	178	49	
MRS3	33S-1	7/25/2013	10.86	43.92	182	49	3.33
MRS3	33S-2	7/29/2013	10.44	40.94	154	44	

a: Fracture test was conducted without self-weight compensation set-up.

b: Specimens did not reach a CMOD larger than 2 mm. G_F and G_f were calculated with available data.

Fracture and Split Tensile Results

The fracture testing further characterizes the concrete mixtures, with the objective of obtaining parameters that may ultimately improve the correlations between mixture parameters and strength, and fatigue and long-term performance. However, with only three different mixes in the current study (and two of those very similar), the mixture parameters contributing to strength and fracture energy are not likely to be differentiated.

The possible correlations of the fracture characterization with the fatigue and full-scale accelerated loading performance of the three mixtures is beyond the scope and length of this paper. However, simply examining the relationships between the parameters obtained from the three methods of testing to single-cycle failure—modulus of rupture, split tensile strength,

fracture energy—provided some interesting results. Figures 2 through 4 compare the parameters from the split tensile and fracture energy testing performed at Penn State to the modulus of rupture testing performed by FAA. All parameters are plotted for all six conditions, that is, the three concrete mixes each under two curing conditions (lab-cured and field-sawn).

In figure 1, the elastic modulus obtained from fracture testing is plotted versus the modulus of rupture. The modulus of rupture and elastic modulus are strongly correlated, except for the results for the MRS2 and MRS3 lab-cured specimens. In figure 2, the tensile strength obtained from split tensile testing of cylinders and cores is plotted versus the modulus of rupture. Surprisingly, the tensile strengths of the lab-cured cylinders for MRS2 and MRS3 did not show losses of strength proportional to the losses in modulus of rupture.

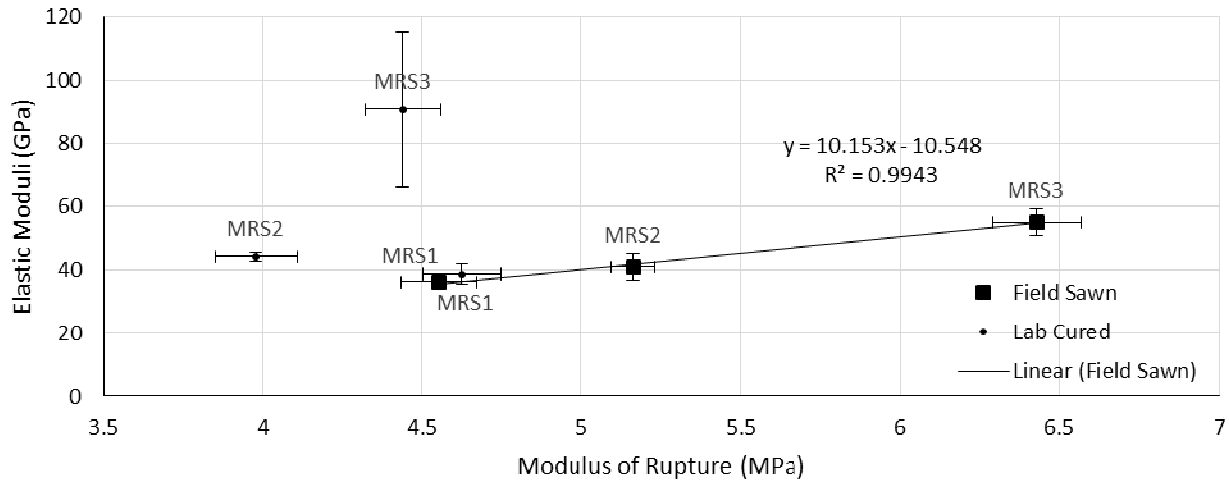


Figure 2. Modulus of rupture (FAA) versus elastic moduli (error bars indicate the standard errors).

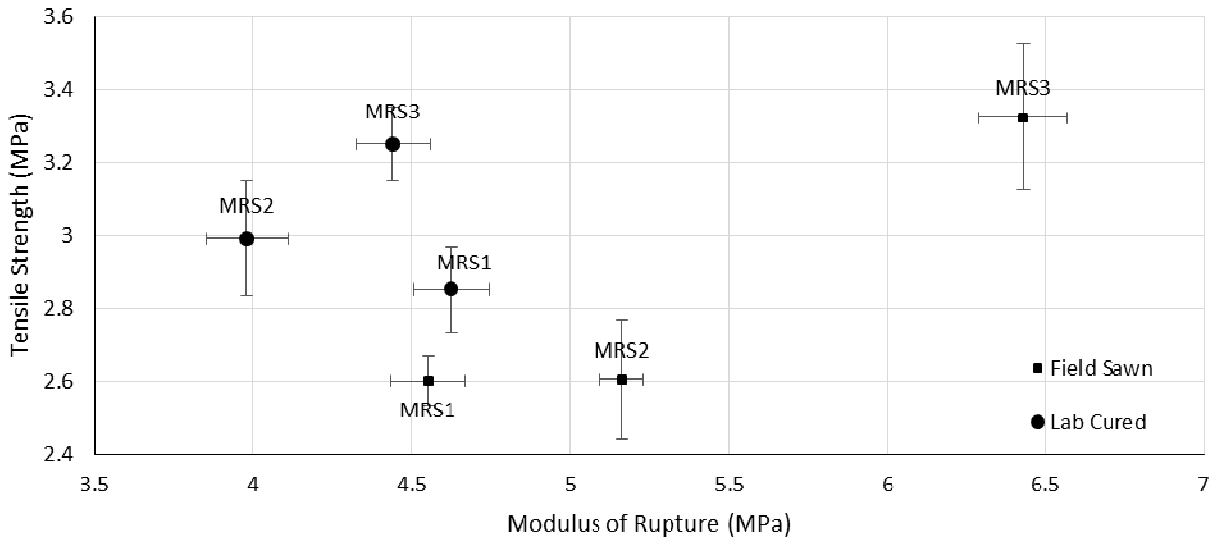


Figure 3. Modulus of rupture (FAA) versus tensile strength (error bars indicate the standard errors).

Finally, in figure 4, both the total fracture energy and the size-effect fracture energy values are plotted versus modulus of rupture. If modulus of rupture and fracture energy are strongly correlated across a variety of mixes, then fracture testing would not further contribute to the long-term fatigue correlations. However, with the limited differences in the CC6 mixes, a correlation was anticipated, particularly for MRS2 and MRS3. The highest total fracture energy values were obtained for the lab-cured beams from MRS2 and MRS3. This is notable, given that the lab-cured beams from MRS2 and MRS3 had been found to have significantly lower modulus of rupture strengths than the field-sawn beams.

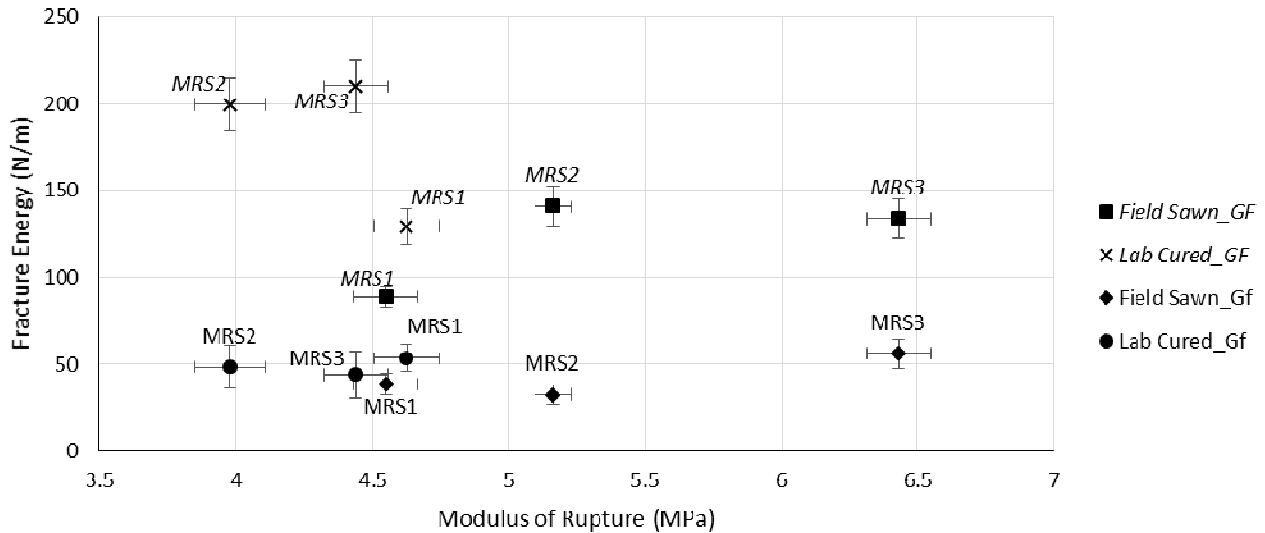


Figure 4. Modulus of rupture (FAA) versus total fracture energy, G_F , and size-effect fracture energy, G_F (error bars indicate the standard errors).

SEM EXAMINATION OF CC6 SPECIMENS

An exploratory use of Scanning Electron Microscopy (SEM) for comparison of the laboratory-cured and field-sawn beams provided for testing from the NAPTF has been conducted. Anomalous results were observed in the routine strength testing of the beam samples from CC6, as documented by Stein (3); after two years of moist curing, the MRS2 and MRS3 beams had been found to have significant drops in flexural strength from 28 days. These discrepancies from well-accepted concrete strength gain patterns occurred in the beams stored for longer terms in high moisture conditions, as compared to the specimens sawed from the full-scale test items. SEM testing may help to identify contributing causes to the observed strength losses over time. The SEM method allows high resolution imaging of the microstructure of a material and can be instrumental for forensic analysis to detect deleterious reactions and their causes.

The specimens for SEM were prepared from the specimens that had been previously used for fracture characterization. The concrete sample size that is tested is approximately $1 \times 1 \times 1 \text{ cm}^3$ and magnifications as high as 50,000X is possible. Energy-dispersive X-ray Spectroscopy (EDS) capability allows identification of the chemical composition of any feature within the image, enabling the analyst to both visualize the damage and to determine the possible causes of damage.

Scanning Electron Microscope (SEM) Sample Preparation

Three test slabs were selected to perform preliminary SEM evaluation based on the availability of field-sawn and lab-cured samples in the lab. For MRS3, slabs 15 N and 17N were selected as both field and lab samples were available. For MRS2, no slab with both field and lab specimens were available; a field-sawn sample from 29S and a lab-cured sample from 29N were used. Following the recommendations of ASTM C1723 (10), small pieces of concrete were extracted from the fractured faces and dried at 85°C for 24 hours. Field-sawn and lab-cured specimens were assembled carefully side-by-side, and epoxied in vacuum condition, and were allowed to set for 24 hours before removing and further processing. Samples were cut using diamond rotary blades, and were polished using 9, 6, 3 and 1 micron sandpapers to achieve a shiny, glossy surface for SEM analysis. These specimens were then carbon coated to avoid charging during the test.

Prepared specimens were tested using FEI Quanta 200 Environmental SEM device, and chemical analyses were performed using Aztec software from Oxford Instruments. Despite carbon coating, some charging occurred during the investigation, which led to using Low Vacuum scanning (which uses water vapor to diminish charges on the surface of samples). This has resulted in slightly lower-quality images in some instances, but all were considered usable.

SEM Specimen 1

This specimen was made from the concrete of slabs 29N and 29S. The lab specimen had very few apparent pores. Figure 5 demonstrates an image of this sample, with a microcrack and a pore. Microcracks in this sample were not frequent, and were mostly associated with formation of ettringite in the pores, which can be an evidence of sulfate attack or delayed ettringite formation, FHWA-RD-01-165 (11). As shown in Figure 5, the needle shaped ettringite formations are completely visible. Ettringite (which is a very expansive substance) may form in the sample as a result of sulfate attack or delayed ettringite formation after curing of the concrete, and has also been noted with repeated wetting and drying cycles by Stark and Bollman (12). It may cause excessive tensile stress in concrete, leading to formation of microcracks and reduction in the strength of the concrete.

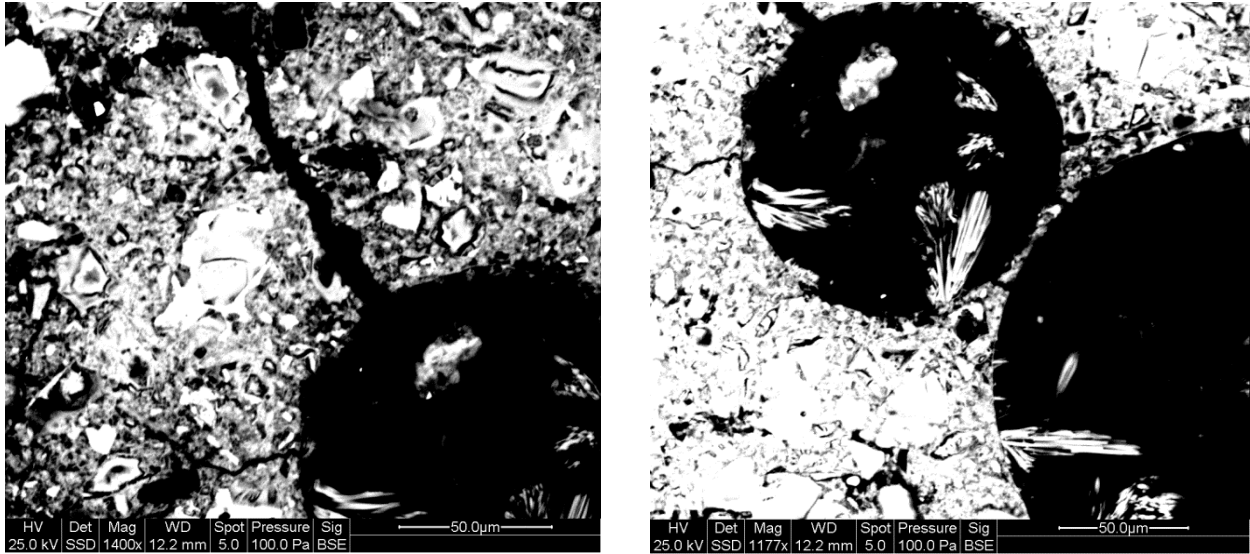


Figure 5. SEM images from MRS2 Slab 29N lab-cured specimen (left) a microcrack and pores; (right) formation of ettringite.

The field specimen had significantly larger pore space distributed throughout the specimen (Figure 6). The field specimen also had the presence of ettringite formations in the pore space (Figure 7). As it can be noticed, cracks are initiated at the pores, where ettringite formations are visible. This trend was visible throughout the specimen, and this can result in significant changes in the properties of concrete.

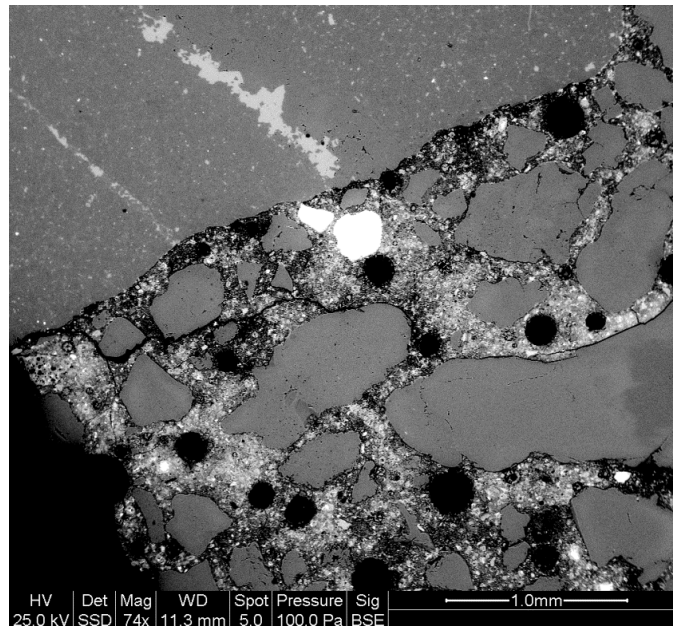


Figure 6. SEM image of pore space distribution in the field-sawn specimen from Slab 29S (MRS2).

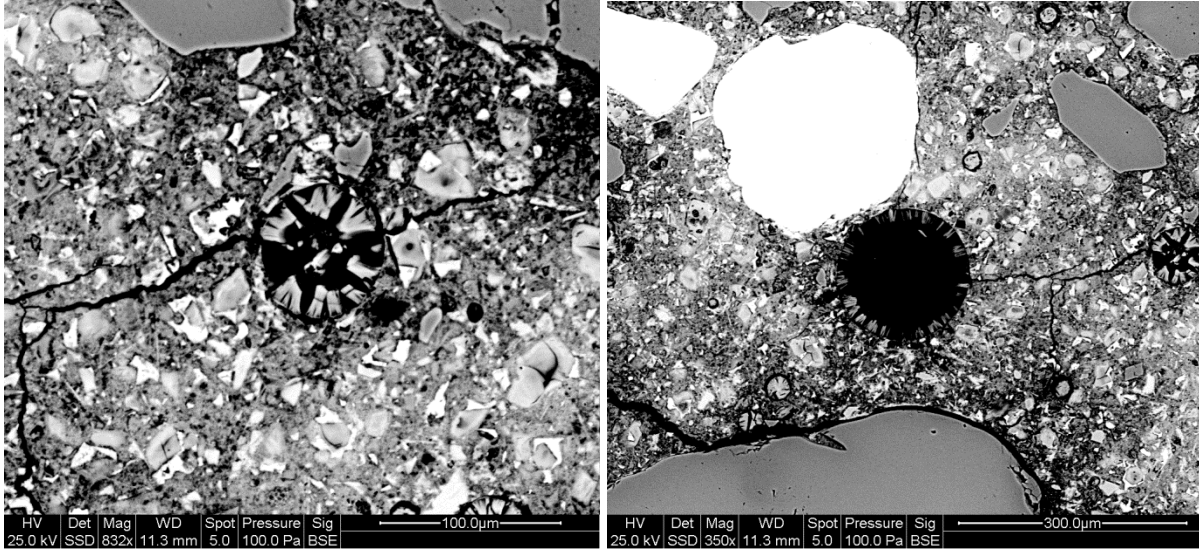


Figure 7. SEM images of ettringite formation in the pore space in in the field-sawn specimen from Slab 29S (MRS2).

SEM Specimen 2

This test specimen consisted of two concrete pieces acquired from the concrete of 15N of CC6. The lab-cured specimen was a relatively consistent sample with voids of different sizes distributed throughout the specimen (Figure 8). There was not severe cracking visible in the specimen upon visual inspection with magnification levels of up to 40X. Cracks began to be visible at zoom levels of around 200X. Some microcracks could be noticed upon further zooming. Unlike the microcracks in specimen 1, these microcracks could not be associated with the presence of pores, and were distributed randomly along the surface of specimen.

EDS was used to analyze the chemical composition of concrete at the crack tips. The bottom right image in Figure 8 indicates a typical part of the field specimen along with the locations of EDS testing zones. Figure 9 shows two sample EDS analysis spectra on the specimen field. The amount of Ca and Si in the tested regions were close (the difference between weight percentage of the two elements can be attributed to the difference in their atomic weight of the elements). This is consistent with the possibility of alkali-silica reactivity (ASR), as noted by Hou (13), but a higher Si content would usually be present. Formation of swelling silica gel can lead to large tensile stresses on the hardened concrete, and results in formation of microcracks. However, no gel was directly observed in the cracks, as shown in Figure 8.

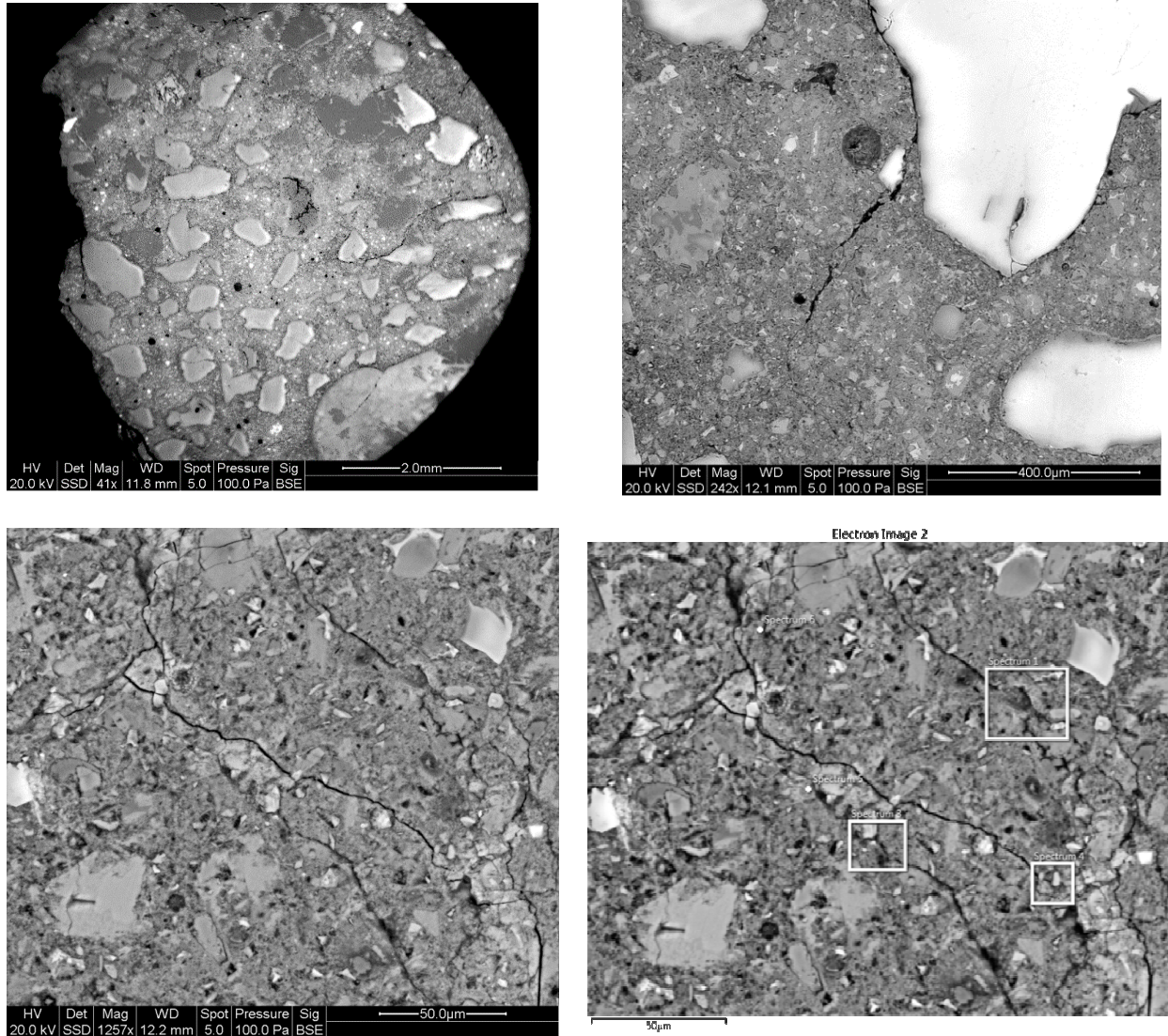


Figure 8. SEM Images from MRS3 Slab 15N lab-cured specimen: (top left) pore size distribution; (top right) cracks; (bottom left) microcracks; (bottom right) microcracks and EDS test locations.

The field-sawn specimen was also tested using SEM in order to find the possible causes of microcracks in the specimen (Figure 10). There are significantly more pores in this specimen. Upon further investigation of this specimen, ettringite formation was also visible inside the pores (Figure 11). These formations were also associated with microcracks.

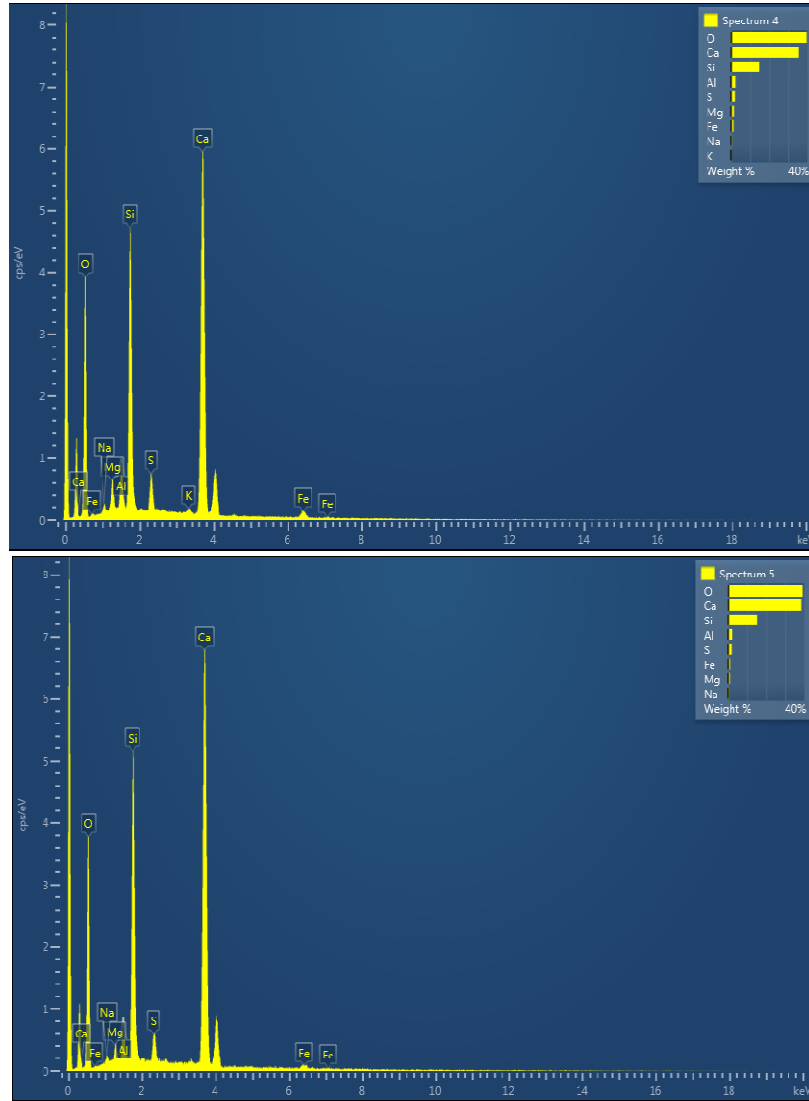


Figure 9. Sample EDS analysis spectra for lab-cured specimen from Slab 15N (MRS3).

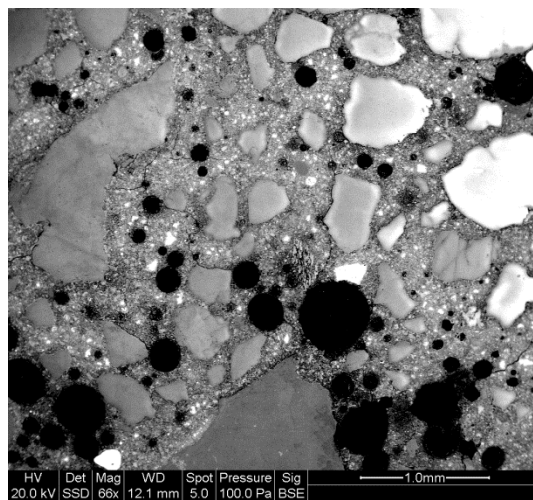


Figure 10. SEM image of pore distribution in the field-sawn specimen from Slab 15N (MRS3).

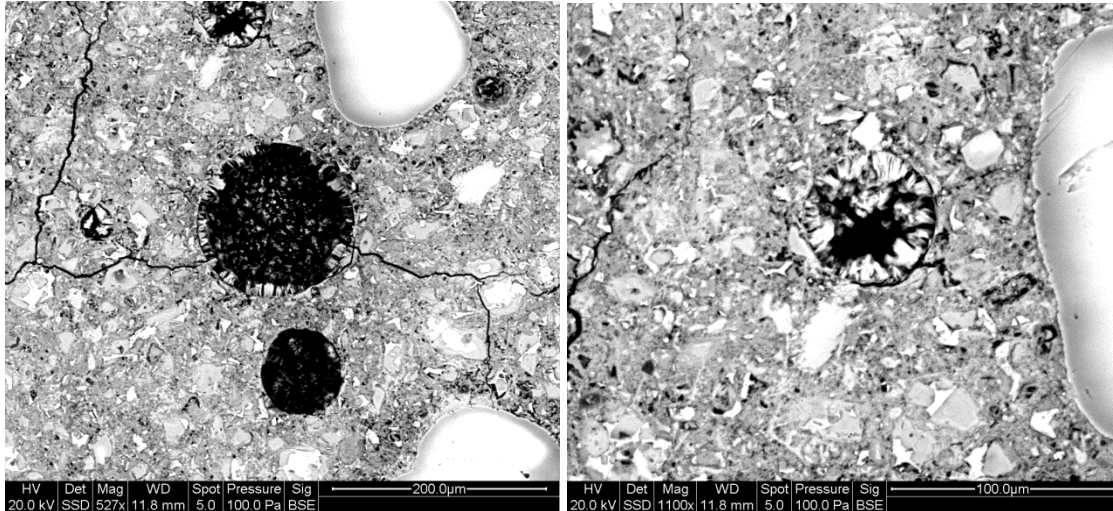


Figure 11. SEM image of ettringite formation in the field-sawn specimen from Slab 15N (MRS3).

SEM Specimen 3

This specimen was acquired from slab 17N of CC6. The lab specimen contained significantly higher pore ratio compared to the previous test specimens (Figure 12). Cracks were randomly formed in this specimen (similar to Specimen 2), and no evidence of ettringite formation was visible in this specimen. Hence, EDS testing was applied to investigate the chemical characterization of the matrix in order to find the possible reasons for microcracking. Figure 8 also shows a sample microcrack in the specimen and zones for performing the EDS analysis on the concrete. EDS analysis spectra on the designated areas again demonstrated similar amounts of Ca and Si, at a ratio of approximately 1.3, which is generally considered too high for ASR.

Study on the field-sawn specimen was also conducted using SEM. As shown in Figure 13, there are more pores in this specimen compared to the lab-cured. However, the differences are not as pronounced as for the previous specimens. Microcracks were also more visible in this specimen, as can be seen in Figure 13. Results of EDS scanning on the field-sawn specimen was similar to that from the lab-cured specimen, and no gel was observed in the cracks.

SEM Summary

Table 4 provides a summary of the observations made from the SEM testing. More pores were observed in the field-sawn specimens. In addition, more ettringite formations were observed in the field-sawn specimens. While the chemical compositions at micro-cracks in both the field-sawn and laboratory-cured specimens were not entirely inconsistent with the conditions for ASR, but all had a lower ratio of Si than would typically be expected with ASR. Gel-filled cracks were not observed.

After the split tensile and fracture testing, specimens were stored in the curing chamber. While the storage time for the field-sawn specimens was much shorter post-testing than the total storage time of the lab-cured specimens, the storage may be obscuring differences between the specimens at the time of testing. Therefore, additional SEM is underway using specimens that were stored under ambient conditions after strength and fracture testing.

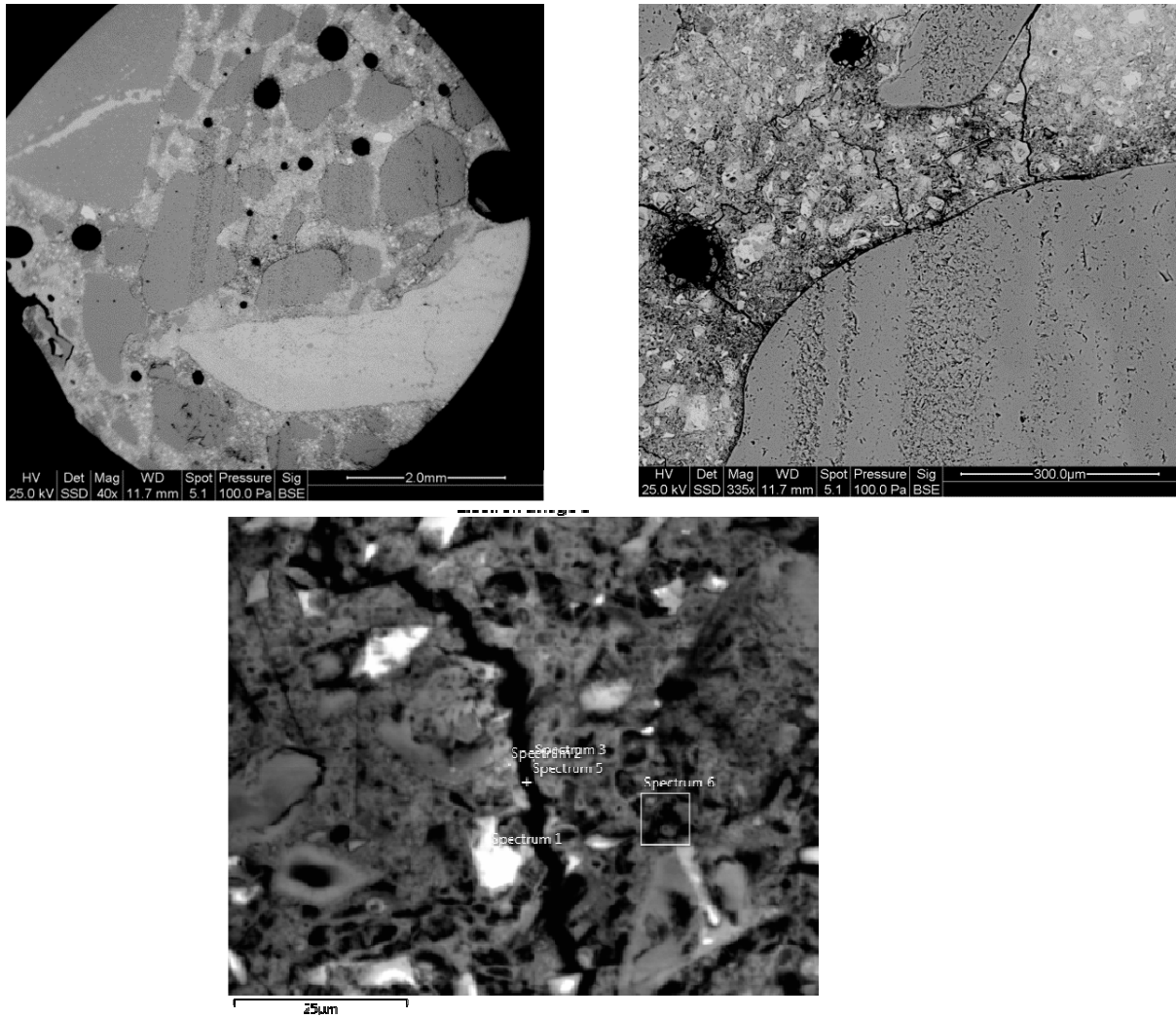


Figure 12. SEM images from MRS3 Slab 17N lab-cured specimen: (top left) pore distribution; (top right) cracks and pores; (bottom) microcracks and EDS test locations.

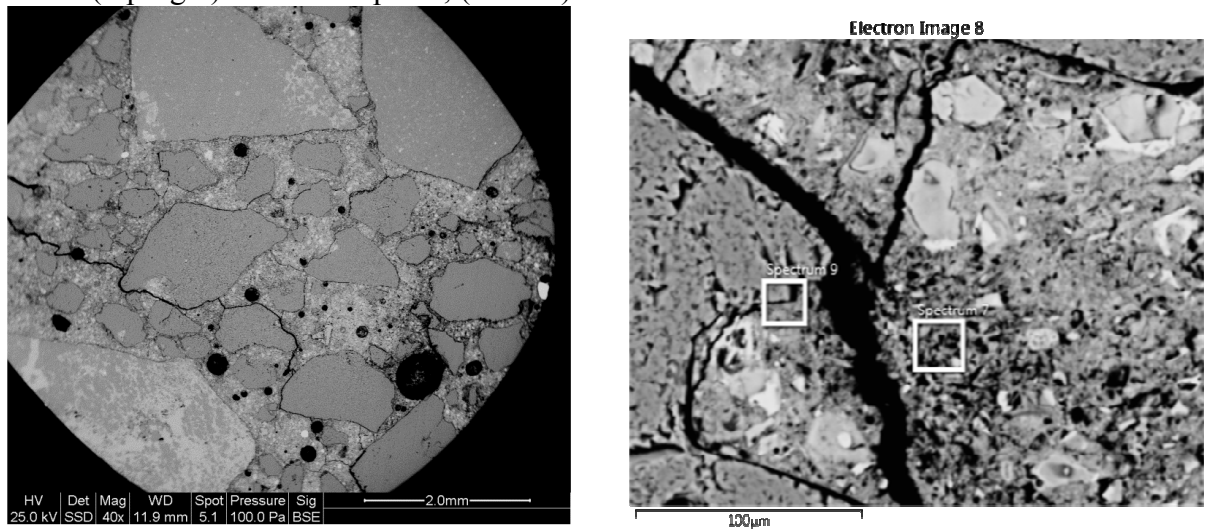


Figure 13. SEM images of field-sawn specimen from MRS3 Slab 17N: (left) pore distribution; (right) microcracks and EDS test locations.

Table 4.
Summary of SEM Observations.

Location	Section ID	Type	SEM/EDS Test Date	Observations
MRS2	29N	Lab-cured	04/09/14	<ul style="list-style-type: none"> • Ettringite formation • Very few apparent pores
MRS2	29S	Field-sawn	04/09/14	<ul style="list-style-type: none"> • Ettringite formation • Significantly larger pore space distributed throughout the specimen
MRS3	15N	Lab-cured	05/12/14	<ul style="list-style-type: none"> • Similar Si and Ca content in EDS analysis • Voids of different size distributed throughout the specimen
MRS3	15N	Field-sawn	05/12/14	<ul style="list-style-type: none"> • Ettringite formation • More pores compared to lab-cured specimen
MRS3	17N	Lab-cured	05/13/14	<ul style="list-style-type: none"> • Similar Si and Ca content in EDS analysis • High amount of pores
MRS3	17N	Field-sawn	05/13/14	<ul style="list-style-type: none"> • Similar Si and Ca content in EDS analysis • Higher amount of pores compared to lab-cured specimen

SUMMARY

The split tensile and fracture testing of the MRS2 and MRS3 laboratory-cured beams and cylinders that was performed at Penn State did not demonstrate the losses observed from the modulus of rupture testing performed by FAA.

Correlations between the material properties obtained from the fracture tests (specifically, peak loads of notched beams, modulus of elasticity of notched beams, size-effect fracture energy G_F , and total fracture energy G_F) and beam flexural strength (MOR) and fatigue behavior of the CC6 mixes (both bench-scale and accelerated loading) are being explored. If complemented with fracture and fatigue testing of additional concrete mixtures in the future, a better correlation to the fatigue behavior might be possible.

SEM examinations of three sets of paired lab-cured and field-sawn concrete specimens were conducted. These examinations would not have predicted the differences in modulus of rupture strength between the lab-cured and field-sawn beams from CC6 MRS2 and MRS3, as observed by FAA. The SEM examinations were performed on samples from the specimens that were tested at Penn State; significant strength losses (in terms of split tensile strength and fracture energy) were also not observed in those specimens.

However, some differences between the specimens were observed. Overall, more pores and ettringite were observed in the field-sawn beams. While the possibility of alkali-silica reactivity could not be excluded, the presence of ASR gel was not observed.

REFERENCES

1. Federal Aviation Administration, 2009, *Airport Pavement Design and Evaluation*, Advisory Circular AC 150/5320-6E, FAA, Washington, D.C.
2. Planas, J., G. V. Guinea, J. C. Gálvez, B. Sanz, and A. M. Fathy, 2007, "Experimental Determination of the Stress-Crack Opening Curve for Concrete in Tension," Final Report of RILEM Technical Committee TC 187-SOC.
3. Stein, J., D. Brill, and C. Ishee, Effects of Long Term Moisture Storage on Concrete Test Samples, 2014 FAA Worldwide Airport Technology Transfer Conference, August 2014.
4. Bazant, Z. P. and K. Xu, 1991, "Size effect in fatigue fracture of concrete," *ACI Materials Journal*, v 88, n 4, p 390-399.
5. Bazant, Z. P. and W. F. Schell, 1993, "Fatigue Fracture of High-Strength Concrete and Size Effect," *ACI Materials Journal*, V. 90, No. 5, pp. 472-477.
6. Zhang, J., V. C. Li and H. Stang, 2001, "Size Effect on Fatigue in Bending of Concrete," *Journal of Materials in Civil Engineering*, Vol. 13, No. 6, American Society of Civil Engineers, pp. 446-453.
7. Shah, S. P., S. E. Swartz and C. Ouyang, 1995, *Fracture Mechanics of Concrete*, John Wiley & Sons.
8. Toumi, A. and A. Bascoul, 2002, "Mode I crack propagation in concrete under fatigue: microscopic observations and modeling," *International Journal for Numerical and Analytical Methods in Geomechanics*, v. 26, pp. 1299-1312.
9. Rocco, C., G. V. Guinea, J. Planas, and M. Elices, 1999, "Size effect and boundary conditions in the Brazilian test: Experimental verification," *Materials and Structures/Materiaux et Constructions*, 32(217), 210-217.
10. ASTM C1723-10, Standard Guide for Examination of Hardened Concrete Using Scanning Electron Microscopy
11. FHWA-RD-01-165, Guidelines for Detection, Analysis, and Treatment of Materials-Related Distress in Concrete Pavements, Federal Highway Administration, 2002.
12. Stark, J. and K. Bollmann, Delayed Ettringite Formation in Concrete, Bahuhaus-University, Weimar, Germany.
13. Hou X, L. J. Struble, R. J. Kirkpatrick, "Formation of ASR gel and the roles of C-S-H and portlandite," *Cement and Concrete Research* 34, March 2004.